Native mass spectrometry reveals binding interactions of SARS-CoV-2 PLpro with inhibitors and ISG15

Virginia K. James[1], Rianna N. Godula[2], Jessica M. Perez[2], Jamie P. Butalewicz[1], Sarah N. Sipe[1], Jon M. Huibregtse[2], Jennifer S. Brodbelt[1*]

[1]Department of Chemistry, The University of Texas at Austin, Austin, TX 78712

[2]Department of Molecular Biosciences, The University of Texas at Austin, Austin, TX 78712

ABSTRACT: Here we used native mass spectrometry (native MS) to probe a SARS-CoV protease, PLpro, which plays critical roles in coronavirus disease by affecting viral protein production and antagonizing host antiviral responses. Ultraviolet photodissociation (UVPD) and variable temperature electrospray ionization (vT ESI) were used to localize binding sites of PLpro inhibitors and revealed the stabilizing effects of inhibitors on protein tertiary structure. We compared PLpro from SARS-CoV-1 and SARS-CoV-2 in terms of inhibitor and ISG15 interactions to discern possible differences in protease function. A PLpro mutant lacking a single cysteine was used to localize inhibitor binding, and thermodynamic measurements revealed that inhibitor PR-619 stabilized the folded PLpro structure. These results will inform further development of PLpro as a therapeutic target against SARS-CoV-2 and other emerging coronaviruses.

Introduction:

SARS-CoV-2 and its numerous variants remain a threat to public health, with over 771 million confirmed disease cases and almost 7 million deaths globally by October 2023.[1] Owing to the magnitude of the COVID pandemic, many new frontiers of viral therapies are being explored.[2] PLpro (papain-like protease) of SARS-CoV-2 is a compelling therapeutic target as it is essential for viral replication and modulation of host antiviral responses.[3] As part of the large non-structural protein domain of coronaviruses,[4] PLpro is required for generation of non-structural proteins nsp1-4 by proteolytic cleavage of the orf1a polyprotein. [5] PLpro is an approximately 36 kDa domain within the much larger nsp3 protein.[6] A second protease, Mpro (nsp5), is similarly essential for proteolytic processing of other viral proteins.[7] In addition to generation of the nsp1-4 proteins, SARS-CoV-2 PLpro modulates host responses by antagonizing the function of ISG15, an interferon-induced ubiquitin-like protein. It does this by catalyzing the cleavage of the isopeptide bond that links the C-terminus of ISG15 to the ?-amino group of lysine side chains of host and viral proteins.[5] Consistent with this dual role of PLpro, the cleavage sites within the orf1a polyprotein bear striking amino acid similarity to the C-terminus of ISG15. Thus, therapeutic inhibition of PLpro would be expected to both disrupt viral protein production and restore the anti-viral activities of ISG15.[8]

Given its importance in disease progression, several avenues for PLpro inhibition have been explored. The active site of PLpro (defined in part by C111, H272, and D286 of the PLpro only domain) may be occupied by small molecules that inhibit protease activity, and several molecules such as GRL-0617[9] and its derivatives[10] have been shown to bind and inhibit PLpro, with x-ray crystal structures of the complexes available in some cases. Structures with other inhibitors, including rac5c and rac3k[11] and several nanomolar-affinity 2-phenylthiophenes compounds, have also been determined.[12] Crystal structures of PLpro•peptide inhibitor complexes have also been solved[13], as well PLpro bound to ISG15[5] as well as ubiquitin and dimeric ubiquitin.[14] Other methods such as nuclear magnetic resonance (NMR) have been used for validation of crystal structures[15] as well as to track PLpro inhibitors that disrupt the interaction between PLpro and ISG15.[9] Biological assays including *in vitro* inhibition experiments have shown successful inhibition of PLpro by many small molecule inhibitors such as 6-thioguanine,[16] PR-619[17] and many others.[18–24] IC_{50} measurements based on monitoring cleavage of the nsp domain site or a polyubiquitin protein in the absence and presence of inhibitors have been widely used to evaluate numerous inhibitors[23,25–28] and nanobodies.[29] As PLpro is a zinc binding protein, it may also be inhibited allosterically by ejection of zinc thus causing protein misfolding,[30] and a recent study found that several small molecule inhibitors can eject zinc from PLpro.[31]

As summarized above, much of the previous work investigating PLpro inhibition has used a variety of conventional biological assays and analytical techniques. Mass spectrometry (MS) has also emerged as a powerful tool for analysis of proteases such as PLpro, affording accurate masses of

cleavage peptides and intact proteins. Liquid chromatography mass spectrometry analysis of tryptic digests of PLpro (i.e., bottom-up proteomics) has shown utility in assays for detecting SARS-CoV-2 via identification of peptides from the virus in complex matrices such as blood and urine,[32] and this method has also localized covalently bound inhibitors to PLpro.[31,33] Crosslinking mass spectrometry revealed that interferon-induced ISG15 protein binds in a different region of PLpro compared to ubiquitin and dimeric ubiquitin.[34] Analysis of intact, denatured PLpro (i.e. top-down proteomics) has been used to differentiate non-covalent and covalently bound inhibitors, especially when multiple inhibitors molecules are bound.[31] While these mass spectrometry techniques involving denatured proteins have been successful in characterizing covalently bound inhibitors, non-covalent interactions are not preserved under denaturing conditions and any information about protein tertiary structure is lost.

Native MS, which involves analyzing proteins in aqueous solutions of high ionic strength, is an attractive alternative as non-covalent interactions may be preserved as proteins are transported to the gas phase by electrospray ionization, allowing retention of protein conformations that resemble solution structures.[35,36,37] Native MS has been applied to numerous structural biology and biophysical investigations related to proteins and macromolecular assemblies, the impact of ligand binding, and thermodynamic properties.[37] The scope of problems that native MS can solve has expanded with the emergence of other auxiliary methods, including collision induced unfolding (CIU) and collision cross section (CCS) measurements,[38–40] variable temperature electrospray ionization (vT-ESI),[41,42] and alternative MS/MS methods,[43] such as ultraviolet photodissociation (UVPD).[44] For example, collision cross section (CCS), a parameter that reflects the shape and size of an ion in the gas phase, has been used to characterize protein conformations[45] and changes that occur upon ligand binding or protein-protein interactions.[46,47] Additionally, changes in CCS can be monitored during low energy collisional activation of protein, a process known as collision induced unfolding (CIU), thus allowing discernment of the impact of ligands on stabilization of proteins.[48–50] vT-ESI allows determination of melting temperatures of proteins and protein complexes[42] and measurement of thermodynamic parameters associated with ligand binding.[51,52] An alternative ion activation method, UVPD has been used to localize inhibitor binding regions of proteins[53] and reveal unfolded/extended vs folded protein regions,[54] thus providing deeper insight into protein tertiary structure.

Coupled with the high mass resolution and high mass accuracy afforded by modern mass spectrometers,[36] these advances in methodologies for native MS have accelerated its adoption for many structural biology studies. Native MS is well suited for examination of interactions between PLpro and inhibitors, particularly those that engage in non-covalent binding,[55] in addition to probing the interactions of PLpro and ISG15. Native MS enables the screening of many inhibitors with only nanogram sample consumption, as shown recently in several studies of Mpro and its small molecule inhibitors[25,26,56–58] or peptide inhibitors.[59] Native MS has also be used to measure the dissociation constant of the M^{pro} dimer,[59] and the effect of inhibitors on the thermodynamic parameters of M^{pro}.[60] Here we showcase the use of native MS to study interactions between PLpro, ISG15, and nsp domain cleavage sites and decipher the effects that small molecule inhibitors have on PLpro activity and tertiary structure stability.

Methods:

Materials

Bovine ubiquitin, and ammonium acetate were purchased from Sigma-Aldrich (St. Louis, MO, USA). LC-MS grade water and methanol was purchased from Merck Millipore (Billerica, MA, USA). For experiments involving native-like charge states, proteins were diluted in a 100 mM ammonium acetate buffer to a final concentration of 10 μM and desalted with Micro Bio-Spin™ P-6 Gel Columns (Bio-Rad Laboratories Inc., Hercules, CA). For experiments with denaturing conditions, proteins were diluted in a denaturing 1:1 water–methanol solution containing 0.1% formic acid to a final concentration of 10 μM without further purification. Small molecule inhibitors were purchased from Cayman Chemicals and used as received. MS1 spectra, structures and masses are shown in **Figures S1-S2** and **Tables S1-S2,** and the MS/MS spectrum of PR-619 is shown in **Figure S3**.

Protein expression and purification

All proteins were generated in house as previously described, with some modifications.[16] The PLpro domain (residues 1-315) was defined as residues 1283 to 1597 of the SARS-CoV-2 ORF1a polyprotein which is equivalent to residues 746 to 1060 of Nsp3. The PLpro domain of SARS-CoV-1 (residues 1-315) was defined as residues 1541-1855 of that SARS-CoV-1 ORF1a polyprotein, which is equivalent to residues 723 to 1037 of Nsp3. All amino acid numbering that follows will be based on the isolated PLpro domains. SARs-CoV-2 PLpro WT and C111S mutant, PLpro from SARS-CoV-1, and Pro-ISG15-HA were purified as GST fusion proteins in BL21 *E. coli*. Overnight cultures were grown at 37 °C for all proteins. Cultures were diluted 1:20 and cultured with shaking for 2 hours at 37 °C. Expression of each protein was induced with 100 μM isopropyl β-D-1-thio-galactopyranoside (IPTG) overnight at 16 °C for all PLpro proteins and 3 hours at 30 °C for Pro-ISG15-HA. Cells were pelleted by centrifugation, resuspended in 10 mL PBS with 0.1% Triton X (Lysing Buffer), and sonicated for 1.5 minutes in 30 second intervals for lysing. Lysates were centrifuged at 10,000 x g for 10 minutes and supernatants were incubated with 100 μL of Glutathione Sepharose (GE Healthcare) and 1 mM phenylmethylsulfonyl (PMSF; Tocris) overnight with end-over-end rotation at 4 °C. Beads were washed three times with Lysis Buffer and three times subsequently with PC Buffer (50 mM Tris, 150 mM NaCl, 0.1% Triton X). Proteins were subjected to site-specific cleavage with PreScission Protease (GE Healthcare) to remove the GST tag. Beads were removed and the protein

concentration in the supernatant was quantified by SDS-PAGE and Western blotting densitometry using a Licor Odyssey Imager. Protein sequences and monoisotopic masses are given in **Table S3**, and monoisotopic masses of expected PLpro1, PLpro2 and PLpro2 C111S complexes are summarized in **Table S4**. Sequence alignment of PLpro1, PLpro2 and PLpro2 C111S is shown in **Figure S4**, and MS1 spectra of native and denatured PLpro is shown in **Figure S5**.

Instrumentation

Most experiments were performed on a Thermo Scientific™ Q Exactive™ HF-X quadrupole-Orbitrap mass spectrometer (Bremen, Germany) with Biopharma option, which was modified to perform ultraviolet photodissociation (UVPD) in the HCD cell by addition of a 500 Hz 193 nm Coherent® ExciStar excimer laser (Santa Cruz, CA) as previously described.[61,62] A variable temperature ESI source was interfaced with the mass spectrometer as previously described, allowing extraction of thermodynamic parameters from Van't Hoff plots created by monitoring the variations in the distribution of protein species as a function of solution temperature.[42,54] Experiments involving some of the solutions containing protein complexes were performed on a prototype Q Exactive Plus Ultra High Mass Range (UHMR) Orbitrap mass spectrometer (Thermo Fisher Scientific, Bremen, Germany), which was optimized for the preservation of weak, non-covalent interactions. Ions were generated by nano electrospray ionization using Au/Pd-coated borosilicate emitters fabricated in-house and using a spray voltage of 0.8-1.2 kV. The C-trap gas pressure was set to 0.5 to 1.0, corresponding to a UHV gauge reading of around 1E-10 to 1.5E-10 mbar, respectively. Throughout the course of this study, some variations in charge state distributions were observed for different solutions or when using the standard nanospray emitters versus the variable temperature source. Replicates of each category of experiment were collected on the same day to minimize these variations.

Data Acquisition and Processing

Variable temperature ESI data was analyzed using a custom MATLAB R2020a script as previously described.[54] UVPD mass spectra were deconvoluted using Xtract in QualBrowser, and sequence coverage maps and fragment abundance plots were generated from the deconvoluted data using MS-TAFI.[63] A custom version of MS-TAFI was used to compare UVPD replicate data so that only fragment ions identified in at least two out of three replicates were retained. Crystal structures were prepared using PyMol (PyMOL Molecular Graphics System, version 2.4 Schrödinger, LLC).

Results and Discussion

SARS-CoV-1 and SARS-CoV-2 PLpro display different affinities for cellular targets

We used native MS to investigate the effects of inhibitors on PLpro and compare the outcomes for PLpro in SARS-CoV-1 (PLpro1) to SARS-CoV-2 (PLpro2). Under native conditions, all three variants of PLpro (PLpro1, PLpro2, and PLpro2 C111S) retained one zinc atom. PLpro from both coronaviruses bind polymeric ubiquitin and ubiquitin-like proteins; PLpro1 has been shown to primarily target diubiquitin while PLpro2 targets the ubiquitin-like interferon-stimulated gene 15 protein (ISG15).[5] Both PLpro1 and PLpro2 bound monomeric ubiquitin with very low affinity (**Figures 1ab, S6-S7**). ISG15 is synthesized as a precursor protein (ProISG15) and is processed by cellular deISGylases and PLpro2 to generate mature ISG15. PLpro2 both processed ProISG15 and bound to mature form of ISG15 (**Figure S8**), as evidenced by formation of high abundance PLpro2•ISG15 complexes (**Figures 1b, S7**), whereas PLpro1 showed no binding to ISG15 (**Figures 1a, S6**). These results agree with prior reports that PLpro1 has lower affinity for ISG15 than PLpro2[64] and that PLpro2 binds ISG15 with higher affinity than binding to ubiquitin.[34] PLpro has 86% sequence conservation between SARS-CoV-1 and SARS-CoV-2 as shown in the sequence alignment in **Figure S5,** and while the catalytic site is conserved between the two viruses, eight amino acids are not conserved in the secondary site of PLpro1 which accounts for the lower affinity of PLpro1 to ISG15.[34,65]

The interaction of PLpro2 and ISG15 was localized by undertaking UVPD of the PLpro2•ISG15 complex, a method which has previously been show to map protein-ligand interactions based on variations in the abundances of fragment ions produced by the apo and holo proteins.[66] In essence, ligand binding results in formation of non-covalent interactions not present for the apo protein, typically leading to suppression of fragmentation of regions involved in the new interactions of the holo protein. It is postulated that non-covalent interactions may be preserved upon UVPD of the holo protein, preventing separation and release of fragment ions even if individual backbone bonds are cleaved. UVPD of the PLpro2•ISG15 complex (14+) resulted in an array of PLpro2 sequence ions as well as ejection of ISG15 (**Figure S9**). There is a broad decrease in abundances of sequence ions corresponding to backbone cleavages near the N- and C- termini of PLpro2 upon UVPD of PLpro2•ISG15 relative to apo PLpro2 (**Figure 1c**). As the active site residues reside near both the C (C111) and N termini (H272, D286) these results agree with the crystal structure of PLpro2•ISG15 (**Figure 1d**), in which ISG15 binds around the active site.

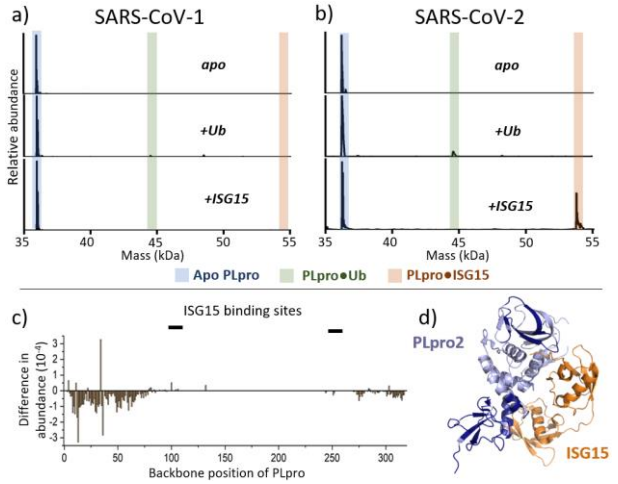

Figure 1. Deconvoluted mass spectra obtained for solutions containing a) PLpro from SARS-CoV-1 and b) SARS-CoV-2 alone (upper), PLpro with ubiquitin (middle), and PLpro with ISG15 (lower). The original non-deconvoluted ESI mass spectra are shown in **Figure S1** for PLpro from SARS-CoV-1 and **Figure S2** for PLpro from Sars-CoV-2. c) Difference in fragmentation of apo PLpro2 and PLpro2•ISG15 based on comparison of abundances of fragment ions originating from backbone cleavages of the protein upon UVPD (1 pulse, 2.5 mJ). Negative values indicate suppression of fragmentation of PLpro2•ISG15 relative to apo PLpro2. d) The crystal structure of PLpro2•ISG15 (PBD 6YVA), where the dark blue regions indicate suppressed fragmentation, and light blue indicate no change or enhanced fragmentation of PLpro2•ISG15 relative to apo PLpro2**.**

Both PLpro1 and PLpro2 bind small inhibitors designed for PLpro2

Although previous studies have extensively evaluated interactions of PLpro1 and PLpro2 with ubiquitin, ubiquitin-like proteins,[34,64] and various small molecule drug candidates,[9,21,25] few studies have compared binding of small molecules to both PLpro1 and PLpro2. We selected seven potential inhibitors, all of which have been evaluated for binding to PLpro2. Solutions containing PLpro2 and each of the small molecule ligands were screened by native MS, and four exhibited low or no binding to PLpro2 (**Figure S10**) and were thus discarded from further analysis. Complexes between PLpro2 and three of the small molecules (GRL-0617, HY-17542, and PR-619) were detected as seen by mass shifts added to PLpro2 in the MS1 spectra (**Figures 2a, S11**). These same small molecules also bound to PLpro1 (**Figure 2b, S12**). The similarity in binding trends for PLpro1 and PLpro2 seems reasonable given that the catalytic triad (C111, H272 and D286) of the active site of PLpro is conserved between the two viruses, and these small molecules are not expected to bind secondary sites on the protein.

Next, we aimed to evaluate the inhibitor binding location and binding mode to PLpro2. The binding site of the most commonly studied inhibitor, GRL-0617, has been localized near the active site of PLpro2 based on several previously solved crystal structures[9], and HY-17542 is expected to bind PLpro in a manner similar to GRL-0617 owing to their nearly identical structures (**Table S1**). Both GRL-0617 and HY-17542 resulted in a mass shift equal to mass of the ligand (**Figure 2a,b**) and bind with high affinity based on the prominence of the PLpro2•ligand complexes relative to apo PLpro2 in the MS1 spectra. For PR-619, PLpro2 (and PLpro1) displayed a mass shift of 170 Da (**Figure 2a,b**) rather than the mass of the intact ligand (223 Da). PR-619 has a unique structural motif containing two thiocyanate groups. Collisional induced dissociation of PR-619 yields fragment ions corresponding to the loss of one or two cyano groups from the thiocyanate motifs, resulting in ions of *m/z* 196 and 170, (**Figure S3).** These results led us to postulate that PR-619 forms one or two disulfide bonds with one or two cysteine residues in PLpro, in each case releasing one cyano group per new disulfide bond.

Although two previous studies evaluated interactions of PR-619 with PLpro and many others have used PR-619 for inhibition of related proteases, such as ubiquitin-specific proteases involved in cancer progression,[67,68] to our knowledge, no study has investigated the binding mechanism or location of PR-619 for deubiquitinating proteases. One important clue is obtained by examination of binding of PR-619 and the C111S mutant of PLpro2. This single point variant lacks the critical C111 in the active site triad, a site that is anticipated to be readily oxidized based on prior crystallographic evidence.[9] This C111S mutant alleviates the question of whether C111 is oxidized or reduced in PLpro2 and removes C111 as a binding site. The mass shift induced by PR-619 binding to PLpro2 C111S is greater (196 Da) than that observed upon PR-619 binding to PLpro1 or PLpro2 (170 Da); this corresponds to the loss of a single cyano group from PR-619 (**Figure 2c, Figure S13**). Because PR-619 loses both cyano groups when binding to PLpro1 and PLpro2, we suspect that PR-619 forms disulfide bonds to C111 and C146, both in close proximity (11 Å^2 by Pymol approximation) in the crystal structure of PLpro (**Figure 2d**). Zinc remains bound to all complexes, suggesting that the four cysteines (C189, C192, C224, C226) that are known to bind zinc are not involved in binding to PR-619. PLpro2 C111S also binds to GRL-0617 and HY-17542, but the proportions of the bound complexes (PLpro2C111S•inhibitor) are lower than observed for either PLpro1 or PLpro2 (**Figure 2c vs Figure 2ab**), indicative of the lower binding affinity of C111S.

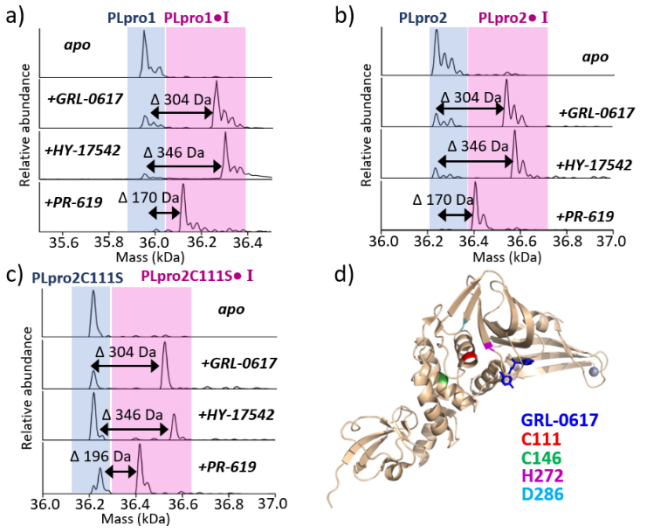

Figure 2. Deconvoluted mass spectra obtained for solutions containing protein alone (10 μM) or with each inhibitor (I, 100 μM) in 100 mM ammonium acetate for a) PLpro1, b) PLpro2, and c) PLpro2 C111S mutant. Non-deconvoluted MS1 spectra are shown in **Figures S11-13** for PLpro1, PLpro2, and PLpro2 C111S, respectively. d) Crystal structure of PLpro2C111S•GRL-0617 (PBD 7CJM, used as a surrogate crystal structure) highlighting the proposed PR-619 binding residues (C111, C146), and the active site (C111, C146, and D286).

The binding modes of each inhibitor were evaluated by two auxiliary mass spectrometry methods. First, collisional heating was used as a means to disassemble the PLpro2•inhibitor complexes. As the voltage applied for in-source collisional activation (i.e. collisional heating) was raised (**Figure S14**), the abundance of each PLpro2•inhibitor complex was monitored. Both GRL-0617 and HY-17542 are dislodged at relatively low collision voltages, an outcome characteristic of non-covalent binding. In contrast, PR-619 is retained by PLpro2 even upon at high collisional voltages, indicative of covalent binding. Second, the survival of the complexes was examined by denaturing the solutions containing PLpro2 after incubation with each inhibitor for 30 minutes and then examining the resulting mass spectra (**Figures S15** and **S16**). As expected, both GRL-0617 and HY-17542 are dislodged in the denaturing solutions (**Figure S15)**, consistent with their non-covalent binding interactions. Some PR-619 remains bound to PLpro2 in the denaturing solution, indicating it is covalently bound (**Figure S16b**). The overall abundance of PLpro2•PR-619 to apo PLpro2 in **Figure S16b** suggests that ~40-50% of the protein is unbound. As also seen in **Figure S16**, the ratio of PLpro2•PR-619 to apo PLpro2 decreases for the higher charge states for the denaturing solutions, indicating that strain from charge-induced protein elongation may further disrupt PR-619 binding despite the inhibitor being covalently bound.

The impact of the inhibitors on the interaction of PLpro2 and ISG15 was also evaluated. Incubation of PLpro2 with ISG15 results in abundant PLpro2•ISG15 complexes (**Figure 3, Figure S17**). All three inhibitors disrupt binding of ISG15 when added to the solutions containing PLpro2 and ISG15 (**Figure 3**). Prior in vitro results have reported inhibition of SARS-CoV-2 in the presence of all three inhibitors including GRL-0617,[9,64] HY-17542,[24] and PR-619[17,25]. A previous NMR study also reported that GRL-0617 out-competed ISG15 to bind to PLpro2 when added to a solution containing PLpro2•ISG15.[9] Despite the differences in binding location and affinity, all inhibitors appear to disrupt binding of PLpro2 to ISG15.

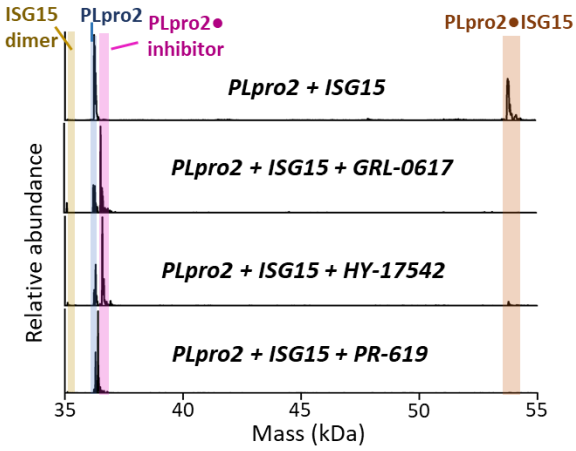

Figure 3. Deconvoluted mass spectra obtained for solutions containing both PLpro2 (10 μM) and ISG15 (10 μM) without or with each inhibitor (100 μM) in 100 mM ammonium acetate. Non-deconvoluted spectra are shown in **Figure S17**.

Inhibitor PR-619 stabilizes PLpro tertiary structure.

To further probe the impact of inhibitor binding on PLpro2, UVPD was used to generate fragmentation patterns of apo PLpro2 and PLpro2• inhibitor complexes. UVPD has been used previously to reveal conformational variations in proteins, as fragmentation is generally enhanced in more flexible and less tightly organized regions. Ligand binding may also contribute to modulation of protein conformations because non-covalent interactions are re-organized during ligand binding. Networks of non-covalent interactions may suppress separation and release of fragment ions, an effect observed as a reduction in the abundances or number of fragment ions upon UVPD. The UVPD mass spectra and sequence maps of PLpro2 and PLpro2•PR-619 are shown in **Figures S18-19**. The number of fragment ions that originate from cleavages of different backbone positions for PLpro2 and PLpro2•PR-619 were counted and plotted as a function of backbone position in **Figure 4**. There was little variation in fragmentation observed upon UVPD of PLpro2 and PLpro2•PR-619 in the absence of supplemental collisional activation (0 V), suggesting similar tertiary structures. In-source collisional activation may be used prior to UVPD to induce protein unfolding,[69] and the resulting fragmentation patterns can be monitored to reveal regions of the protein that are disrupted.[54] While UVPD of PLpro2•PR-619 after no or low in-source collision activation resulted in insignificant differences in fragmentation compared to apo PLpro2, fragmentation increased in the region spanning

K105 to N146 after greater in-source collisional activation (200 V). This region of enhanced fragmentation is demarcated on the sequence shown in **Figure 4b** and shaded on the crystal structure in **Figure 4c** and encompasses the suspected PR-619 binding site. This suppression of UVPD fragmentation that emerges with higher values of in-source collisional activation indicate that PR-619 may stabilize the mid-section of PLpro. This outcome is also consistent with the potential crosslinking mode of PR-619 which would require cleavage of two bonds to produce sequence ions originated from backbone cleavages spanning C111 and C146. The possibility that PR-619 staples PLpro and/or stabilizes the PLpro structure is probed in more detail as a function of solution temperature in the next section. The two non-covalent inhibitors, GRL-0617 and HY-17542, are released from PLpro2 upon in-source collisional activation or during transfer to the collision cell (**Figure S14**), thus information about binding sites cannot be obtained by UVPD for these weakly bound inhibitors.

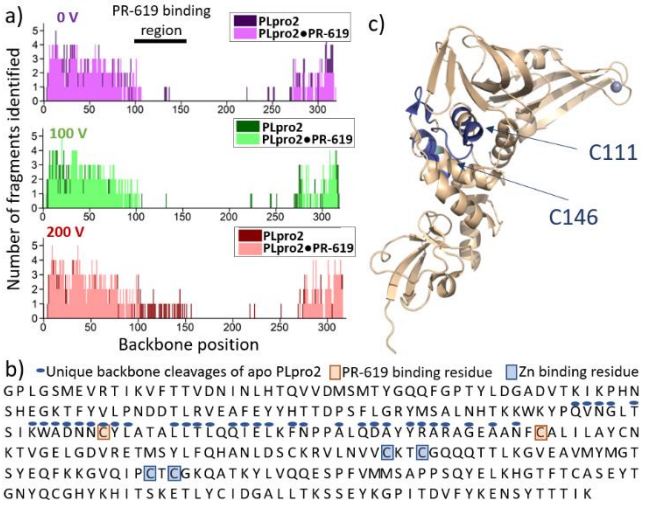

Figure 4. a) Number of sequence ions originating from cleavages of each backbone position of apo PLpro2 (10+) and PLpro2•PR-619 (10+) upon UVPD (1 pulse, 2.5 mJ) when using 0, 100, or 200 V of in-source collisional activation. The lighter colored bars representing the fragmentation of PLpro2•PR-619 are placed in front of the darker bars for apo PLpro2, allowing better visualization of those regions for which fragmentation of PLpro2•PR-619 is suppressed relative to PLpro2. The backbone cleavage sites identified for apo PLpro2 that were not identified for PLpro2•PR-619 are (b) marked with blue dashes on the sequence map and (c) shaded in blue on the crystal structure (PDB 7CJM), indicating regions where fragmentation is suppressed in the PLpro2•PR-619 complex.

Variable temperature ESI (vT-ESI) analysis of apo PLpro2 and PLpro2•PR-619 was undertaken to evaluate variations in the thermodynamic parameters of PLpro2 upon PR-619 binding and probe structural stabilization imparted by inhibitor binding. For this method, the charge state distributions of the protein are monitored as a function of the temperature of the solution (**Figure 5a**) and used to generate melting curves (**Figure 5b**) and Van't Hoff plots (**Figure S20**) from which ΔG, ΔH, and ΔS are determined (**Figure 5c**). vT-ESI of apo PLpro2 shows that the protein retains zinc even at high temperatures, suggesting that zinc is strongly bound (**Figure 5a**). Zinc is only lost when the protein is sprayed from denaturing solutions (**Figure S15, 16**). The vT-ESI data shows that apo PLpro2 shifts to higher charge states as the temperature increases, consistent with protein elongation/unfolding which facilitates protonation of more basic sites. In contrast, PLpro•PR-619 shows less variation in its charge state distribution as a function of solution temperature, indicative of greater stability of the folded PLpro2•PR-619 complex (**Figure 5a, b**). Thermodynamic analysis of apo PLpro2 vs PLpro2•PR-619 reveals that unfolding of apo PLpro2 is entropically favorable whereas unfolding of PLpro2•PR-619 is enthalpically favorable (**Figures 5c, S20**). Enthalpically favorability of the thermal denaturation of PLpro2•PR-619 corresponds to an increase of intermolecular interactions which outweighs the restriction in entropy. These results affirm that PR-619 stabilizes the tertiary structure of PLpro2, which is congruent with a crosslinking binding mode.

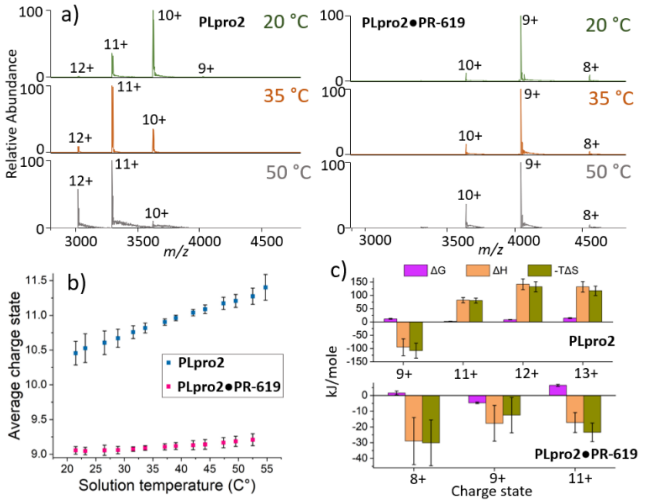

Figure 5. a) MS1 spectra of solutions containing PLpro2 (10 μM in 100 mM ammonium acetate) or PLpro2•PR-619 (10 μm protein and 100 μm ligand in 100 mM ammonium acetate) at 20, 35, and 50 °C, from which b) melting curves for apo PLpro2 and PLpro2•PR-619. c) From the melting curves, van't Hoff plots were determined (**Figure S20**) and used to calculate thermodynamic values.

Conclusions:

To distinguish differences in function and inhibition of PLpro from SARS-CoV-1 and SARS-CoV-2, we used native MS to compare the binding affinities of two PLpro proteins (PLpro1 and PLpro2, respectively) to cellular targets (ISG15) as well as small molecular inhibitors previously designed for PLpro2. We confirmed that PLpro2 preferentially binds to ISG15 relative to PLpro1. At the same time, PLpro1 bound inhibitors designed for PLpro2. These results suggest that despite the differences in sequence conservation of PLpro between coronaviruses, the protease may still be a

good therapeutic target for a broad range of coronaviruses. The effects of inhibitor binding on protein tertiary structural stability were probed with variable temperature ESI and UVPD. We used ultraviolet photodissociation and a PLpro C111S mutant to localize the binding of PR-619, an inhibitor highlighted in several recent PLpro studies. We found that PR-619 acts as a crosslinker, stabilizing the tertiary structure of PLpro as supported by vT-ESI results. These results suggest that PR-619, a general inhibitor of deubiquitylating enzymes (DUBs), may inhibit these enzymes by a similar mechanism.

ASSOCIATED CONTENT

Supporting Information. Sequences, masses, and raw mass spectra for proteins, protein complexes, and inhibitors, sequence alignment for all PLpro proteins, UVPD data and identified fragment ions, and van't Hoff plots.

AUTHOR INFORMATION

Corresponding Author

* Jennifer S. Brodbelt
Email: jbrodbelt@cm.utexas.edu

Funding Sources

Funding from the National Institutes of Health (R35GM13965) and the Robert A. Welch Foundation (F-1155) to J.S.B. is gratefully acknowledged. This work was supported by a grant from the National Institutes for Allergy and Infectious Diseases (AI096090) to J.M.H.

REFERENCES

(1) *WHO Coronavirus (COVID-19) Dashboard*. https://covid19.who.int (accessed 2023-10-27).

(2) Li, G.; Hilgenfeld, R.; Whitley, R.; De Clercq, E. Therapeutic Strategies for COVID-19: Progress and Lessons Learned. *Nat Rev Drug Discov* **2023**, *22* (6), 449–475. https://doi.org/10.1038/s41573-023-00672-y.

(3) McClain, C. B.; Vabret, N. SARS-CoV-2: The Many Pros of Targeting PLpro. *Sig Transduct Target Ther* **2020**, *5* (1), 1–2. https://doi.org/10.1038/s41392-020-00335-z.

(4) Jahirul Islam, Md.; Nawal Islam, N.; Siddik Alom, Md.; Kabir, M.; Halim, M. A. A Review on Structural, Non-Structural, and Accessory Proteins of SARS-CoV-2: Highlighting Drug Target Sites. *Immunobiology* **2023**, *228* (1), 152302. https://doi.org/10.1016/j.imbio.2022.152302.

(5) Shin, D.; Mukherjee, R.; Grewe, D.; Bojkova, D.; Baek, K.; Bhattacharya, A.; Schulz, L.; Widera, M.; Mehdipour, A. R.; Tascher, G.; Geurink, P. P.; Wilhelm, A.; van der Heden van Noort, G. J.; Ovaa, H.; Müller, S.; Knobeloch, K.-P.; Rajalingam, K.; Schulman, B. A.; Cinatl, J.; Hummer, G.; Ciesek, S.; Dikic, I. Papain-like Protease Regulates SARS-CoV-2 Viral Spread and Innate Immunity. *Nature* **2020**, *587* (7835), 657–662. https://doi.org/10.1038/s41586-020-2601-5.

(6) Amin, Sk. A.; Banerjee, S.; Ghosh, K.; Gayen, S.; Jha, T. Protease Targeted COVID-19 Drug Discovery and Its Challenges: Insight into Viral Main Protease (Mpro) and Papain-like Protease (PLpro) Inhibitors. *Bioorganic & Medicinal Chemistry* **2021**, *29*, 115860. https://doi.org/10.1016/j.bmc.2020.115860.

(7) Hu, Q.; Xiong, Y.; Zhu, G.-H.; Zhang, Y.-N.; Zhang, Y.-W.; Huang, P.; Ge, G.-B. The SARS-CoV-2 Main Protease (Mpro): Structure, Function, and Emerging Therapies for COVID-19. *MedComm* **2022**, *3* (3), e151. https://doi.org/10.1002/mco2.151.

(8) Liu, G.; Lee, J.-H.; Parker, Z. M.; Acharya, D.; Chiang, J. J.; van Gent, M.; Riedl, W.; Davis-Gardner, M. E.; Wies, E.; Chiang, C.; Gack, M. U. ISG15-Dependent Activation of the Sensor MDA5 Is Antagonized by the SARS-CoV-2 Papain-like Protease to Evade Host Innate Immunity. *Nat Microbiol* **2021**, *6* (4), 467–478. https://doi.org/10.1038/s41564-021-00884-1.

(9) Fu, Z.; Huang, B.; Tang, J.; Liu, S.; Liu, M.; Ye, Y.; Liu, Z.; Xiong, Y.; Zhu, W.; Cao, D.; Li, J.; Niu, X.; Zhou, H.; Zhao, Y. J.; Zhang, G.; Huang, H. The Complex Structure of GRL0617 and SARS-CoV-2 PLpro Reveals a Hot Spot for Antiviral Drug Discovery. *Nat Commun* **2021**, *12* (1), 488. https://doi.org/10.1038/s41467-020-20718-8.

(10) Sanders, B. C.; Pokhrel, S.; Labbe, A. D.; Mathews, I. I.; Cooper, C. J.; Davidson, R. B.; Phillips, G.; Weiss, K. L.; Zhang, Q.; O'Neill, H.; Kaur, M.; Schmidt, J. G.; Reichard, W.; Surendranathan, S.; Parvathareddy, J.; Phillips, L.; Rainville, C.; Sterner, D. E.; Kumaran, D.; Andi, B.; Babnigg, G.; Moriarty, N. W.; Adams, P. D.; Joachimiak, A.; Hurst, B. L.; Kumar, S.; Butt, T. R.; Jonsson, C. B.; Ferrins, L.; Wakatsuki, S.; Galanie, S.; Head, M. S.; Parks, J. M. Potent and Selective Covalent Inhibition of the Papain-like Protease from SARS-CoV-2. *Nat Commun* **2023**, *14* (1), 1733. https://doi.org/10.1038/s41467-023-37254-w.

(11) Calleja, D. J.; Kuchel, N.; Lu, B. G. C.; Birkinshaw, R. W.; Klemm, T.; Doerflinger, M.; Cooney, J. P.; Mackiewicz, L.; Au, A. E.; Yap, Y. Q.; Blackmore, T. R.; Katneni, K.; Crighton, E.; Newman, J.; Jarman, K. E.; Call, M. J.; Lechtenberg, B. C.; Czabotar, P. E.; Pellegrini, M.; Charman, S. A.; Lowes, K. N.; Mitchell, J. P.; Nachbur, U.; Lessene, G.; Komander, D. Insights Into Drug Repurposing, as Well as Specificity and Compound Properties of Piperidine-Based SARS-CoV-2 PLpro Inhibitors. *Frontiers in Chemistry* **2022**, *10*.

(12) Shen, Z.; Ratia, K.; Cooper, L.; Kong, D.; Lee, H.; Kwon, Y.; Li, Y.; Alqarni, S.; Huang, F.; Dubrovskyi, O.; Rong, L.; Thatcher, G. R. J.; Xiong, R. Design of SARS-CoV-2 PLpro Inhibitors for COVID-19 Antiviral Therapy Leveraging Binding Cooperativity. *J. Med. Chem.* **2022**, *65* (4), 2940–2955. https://doi.org/10.1021/acs.jmedchem.1c01307.

(13) Rut, W.; Lv, Z.; Zmudzinski, M.; Patchett, S.; Nayak, D.; Snipas, S. J.; El Oualid, F.; Huang, T. T.; Bekes, M.; Drag, M.; Olsen, S. K. Activity Profiling and Crystal Structures of Inhibitor-Bound SARS-CoV-2 Papain-like Protease: A Framework for Anti–COVID-19 Drug Design. *Science Advances* **2020**, *6* (42), eabd4596. https://doi.org/10.1126/sciadv.abd4596.

(14) Vliet, V. J. E. van; Huynh, N.; Palà, J.; Patel, A.; Singer, A.; Slater, C.; Chung, J.; Huizen, M. van; Teyra, J.; Miersch, S.; Luu, G.-K.; Ye, W.; Sharma, N.; Ganaie, S. S.; Russell, R.; Chen, C.; Maynard, M.; Amarasinghe, G. K.; Mark, B. L.; Kikkert, M.; Sidhu, S. S. Ubiquitin Variants Potently Inhibit SARS-CoV-2 PLpro and Viral Replication via a Novel Site Distal to the

Protease Active Site. *PLOS Pathogens* **2022**, *18* (12), e1011065. https://doi.org/10.1371/journal.ppat.1011065.

(15) Napolitano, V.; Dabrowska, A.; Schorpp, K.; Mourão, A.; Barreto-Duran, E.; Benedyk, M.; Botwina, P.; Brandner, S.; Bostock, M.; Chykunova, Y.; Czarna, A.; Dubin, G.; Fröhlich, T.; Hölscher, M.; Jedrysik, M.; Matsuda, A.; Owczarek, K.; Pachota, M.; Plettenburg, O.; Potempa, J.; Rothenaigner, I.; Schlauderer, F.; Slysz, K.; Szczepanski, A.; Greve-Isdahl Mohn, K.; Blomberg, B.; Sattler, M.; Hadian, K.; Popowicz, G. M.; Pyrc, K. Acriflavine, a Clinically Approved Drug, Inhibits SARS-CoV-2 and Other Betacoronaviruses. *Cell Chemical Biology* **2022**, *29* (5), 774-784.e8. https://doi.org/10.1016/j.chembiol.2021.11.006.

(16) Swaim, C. D.; Dwivedi, V.; Perng, Y.-C.; Zhao, X.; Canadeo, L. A.; Harastani, H. H.; Darling, T. L.; Boon, A. C. M.; Lenschow, D. J.; Kulkarni, V.; Huibregtse, J. M. 6-Thioguanine Blocks SARS-CoV-2 Replication by Inhibition of PLpro. *iScience* **2021**, *24* (10), 103213. https://doi.org/10.1016/j.isci.2021.103213.

(17) Große, M.; Setz, C.; Rauch, P.; Auth, J.; Morokutti-Kurz, M.; Temchura, V.; Schubert, U. Inhibitors of Deubiquitinating Enzymes Interfere with the SARS-CoV-2 Papain-like Protease and Block Virus Replication In Vitro. *Viruses* **2022**, *14* (7), 1404. https://doi.org/10.3390/v14071404.

(18) Narayanan, A.; Narwal, M.; Majowicz, S. A.; Varricchio, C.; Toner, S. A.; Ballatore, C.; Brancale, A.; Murakami, K. S.; Jose, J. Identification of SARS-CoV-2 Inhibitors Targeting Mpro and PLpro Using in-Cell-Protease Assay. *Commun Biol* **2022**, *5* (1), 1–17. https://doi.org/10.1038/s42003-022-03090-9.

(19) Protić, S.; Kaličanin, N.; Sencanski, M.; Prodanović, O.; Milicevic, J.; Perovic, V.; Paessler, S.; Prodanović, R.; Glisic, S. In Silico and In Vitro Inhibition of SARS-CoV-2 PLpro with Gramicidin D. *International Journal of Molecular Sciences* **2023**, *24* (3), 1955. https://doi.org/10.3390/ijms24031955.

(20) Lewis, D. S. M.; Ho, J.; Wills, S.; Kawall, A.; Sharma, A.; Chavada, K.; Ebert, M. C. C. J. C.; Evoli, S.; Singh, A.; Rayalam, S.; Mody, V.; Taval, S. Aloin Isoforms (A and B) Selectively Inhibits Proteolytic and Deubiquitinating Activity of Papain like Protease (PLpro) of SARS-CoV-2 in Vitro. *Sci Rep* **2022**, *12* (1), 2145. https://doi.org/10.1038/s41598-022-06104-y.

(21) Kulandaisamy, R.; Kushwaha, T.; Dalal, A.; Kumar, V.; Singh, D.; Baswal, K.; Sharma, P.; Praneeth, K.; Jorwal, P.; Kayampeta, S. R.; Sharma, T.; Maddur, S.; Kumar, M.; Kumar, S.; Polamarasetty, A.; Singh, A.; Sehgal, D.; Gholap, S. L.; Appaiahgari, M. B.; Katika, M. R.; Inampudi, K. K. Repurposing of FDA Approved Drugs Against SARS-CoV-2 Papain-Like Protease: Computational, Biochemical, and in Vitro Studies. *Front Microbiol* **2022**, *13*, 877813. https://doi.org/10.3389/fmicb.2022.877813.

(22) Loffredo, M.; Lucero, H.; Chen, D.-Y.; O'Connell, A.; Bergqvist, S.; Munawar, A.; Bandara, A.; De Graef, S.; Weeks, S. D.; Douam, F.; Saeed, M.; Munawar, A. H. The In-Vitro Effect of Famotidine on SARS-CoV-2 Proteases and Virus Replication. *Sci Rep* **2021**, *11* (1), 5433. https://doi.org/10.1038/s41598-021-84782-w.

(23) Klemm, T.; Ebert, G.; Calleja, D. J.; Allison, C. C.; Richardson, L. W.; Bernardini, J. P.; Lu, B. G.; Kuchel, N. W.; Grohmann, C.; Shibata, Y.; Gan, Z. Y.; Cooney, J. P.; Doerflinger, M.; Au, A. E.; Blackmore, T. R.; van der Heden van Noort, G. J.; Geurink, P. P.; Ovaa, H.; Newman, J.; Riboldi-Tunnicliffe, A.; Czabotar, P. E.; Mitchell, J. P.; Feltham, R.; Lechtenberg, B. C.; Lowes, K. N.; Dewson, G.; Pellegrini, M.; Lessene, G.; Komander, D. Mechanism and Inhibition of the Papain-like Protease, PLpro, of SARS-CoV-2. *The EMBO Journal* **2020**, *39* (18), e106275. https://doi.org/10.15252/embj.2020106275.

(24) Cho, H.; Kim, Y. J.; Chae, J.-W.; Meyer, M. R.; Kim, S. K.; Ryu, C. S. In Vitro Metabolic Characterization of the SARS-CoV-2 Papain-like Protease Inhibitors GRL0617 and HY-17542. *Frontiers in Pharmacology* **2023**, *14*.

(25) Cho, C.-C.; Li, S. G.; Lalonde, T. J.; Yang, K. S.; Yu, G.; Qiao, Y.; Xu, S.; Ray Liu, W. Drug Repurposing for the SARS-CoV-2 Papain-Like Protease. *ChemMedChem* **2022**, *17* (1), e202100455. https://doi.org/10.1002/cmdc.202100455.

(26) Ma, C.; Hu, Y.; Townsend, J. A.; Lagarias, P. I.; Marty, M. T.; Kolocouris, A.; Wang, J. Ebselen, Disulfiram, Carmofur, PX-12, Tideglusib, and Shikonin Are Nonspecific Promiscuous SARS-CoV-2 Main Protease Inhibitors. *ACS Pharmacol. Transl. Sci.* **2020**, *3* (6), 1265–1277. https://doi.org/10.1021/acsptsci.0c00130.

(27) Freitas, B. T.; Durie, I. A.; Murray, J.; Longo, J. E.; Miller, H. C.; Crich, D.; Hogan, R. J.; Tripp, R. A.; Pegan, S. D. Characterization and Noncovalent Inhibition of the Deubiquitinase and deISGylase Activity of SARS-CoV-2 Papain-Like Protease. *ACS Infect. Dis.* **2020**, *6* (8), 2099–2109. https://doi.org/10.1021/acsinfecdis.0c00168.

(28) Zhao, Y.; Du, X.; Duan, Y.; Pan, X.; Sun, Y.; You, T.; Han, L.; Jin, Z.; Shang, W.; Yu, J.; Guo, H.; Liu, Q.; Wu, Y.; Peng, C.; Wang, J.; Zhu, C.; Yang, X.; Yang, K.; Lei, Y.; Guddat, L. W.; Xu, W.; Xiao, G.; Sun, L.; Zhang, L.; Rao, Z.; Yang, H. High-Throughput Screening Identifies Established Drugs as SARS-CoV-2 PLpro Inhibitors. *Protein Cell* **2021**, *12* (11), 877–888. https://doi.org/10.1007/s13238-021-00836-9.

(29) Armstrong, L. A.; Lange, S. M.; Cesare, V. D.; Matthews, S. P.; Nirujogi, R. S.; Cole, I.; Hope, A.; Cunningham, F.; Toth, R.; Mukherjee, R.; Bojkova, D.; Gruber, F.; Gray, D.; Wyatt, P. G.; Cinatl, J.; Dikic, I.; Davies, P.; Kulathu, Y. Biochemical Characterization of Protease Activity of Nsp3 from SARS-CoV-2 and Its Inhibition by Nanobodies. *PLOS ONE* **2021**, *16* (7), e0253364. https://doi.org/10.1371/journal.pone.0253364.

(30) Maiti, B. K. Can Papain-like Protease Inhibitors Halt SARS-CoV-2 Replication? *ACS Pharmacol. Transl. Sci.* **2020**, *3* (5), 1017–1019. https://doi.org/10.1021/acsptsci.0c00093.

(31) Sargsyan, K.; Lin, C.-C.; Chen, T.; Grauffel, C.; Chen, Y.-P.; Yang, W.-Z.; S. Yuan, H.; Lim, C. Multi-Targeting of Functional Cysteines in Multiple Conserved SARS-CoV-2 Domains by Clinically Safe Zn-Ejectors. *Chemical Science* **2020**, *11* (36), 9904–9909. https://doi.org/10.1039/D0SC02646H.

(32) Lima, N. M.; Fernandes, B. L. M.; Alves, G. F.; de Souza, J. C. Q.; Siqueira, M. M.; Patrícia do Nascimento, M.; Moreira, O. B. O.; Sussulini, A.; de Oliveira, M. A. L. Mass Spectrometry Applied to Diagnosis, Prognosis, and Therapeutic Targets Identification for the Novel Coronavirus

SARS-CoV-2: A Review. *Analytica Chimica Acta* **2022**, *1195*, 339385. https://doi.org/10.1016/j.aca.2021.339385.

(33) Yu, W.; Zhao, Y.; Ye, H.; Wu, N.; Liao, Y.; Chen, N.; Li, Z.; Wan, N.; Hao, H.; Yan, H.; Xiao, Y.; Lai, M. Structure-Based Design of a Dual-Targeted Covalent Inhibitor Against Papain-like and Main Proteases of SARS-CoV-2. *J. Med. Chem.* **2022**, *65* (24), 16252–16267. https://doi.org/10.1021/acs.jmedchem.2c00954.

(34) Wydorski, P. M.; Osipiuk, J.; Lanham, B. T.; Tesar, C.; Endres, M.; Engle, E.; Jedrzejczak, R.; Mullapudi, V.; Michalska, K.; Fidelis, K.; Fushman, D.; Joachimiak, A.; Joachimiak, L. A. Dual Domain Recognition Determines SARS-CoV-2 PLpro Selectivity for Human ISG15 and K48-Linked Di-Ubiquitin. *Nat Commun* **2023**, *14* (1), 2366. https://doi.org/10.1038/s41467-023-38031-5.

(35) Jooß, K.; McGee, J. P.; Kelleher, N. L. Native Mass Spectrometry at the Convergence of Structural Biology and Compositional Proteomics. *Acc. Chem. Res.* **2022**, *55* (14), 1928–1937. https://doi.org/10.1021/acs.accounts.2c00216.

(36) Tamara, S.; den Boer, M. A.; Heck, A. J. R. High-Resolution Native Mass Spectrometry. *Chem. Rev.* **2022**, *122* (8), 7269–7326. https://doi.org/10.1021/acs.chemrev.1c00212.

(37) Webb, I. K. Recent Technological Developments for Native Mass Spectrometry. *Biochimica et Biophysica Acta (BBA) - Proteins and Proteomics* **2022**, *1870* (1), 140732. https://doi.org/10.1016/j.bbapap.2021.140732.

(38) Pukala, T. Importance of Collision Cross Section Measurements by Ion Mobility Mass Spectrometry in Structural Biology. *Rapid Communications in Mass Spectrometry* **2019**, *33* (S3), 72–82. https://doi.org/10.1002/rcm.8294.

(39) Dixit, S. M.; Polasky, D. A.; Ruotolo, B. T. Collision Induced Unfolding of Isolated Proteins in the Gas Phase: Past, Present, and Future. *Current Opinion in Chemical Biology* **2018**, *42*, 93–100. https://doi.org/10.1016/j.cbpa.2017.11.010.

(40) Ruotolo, B. T. Collision Cross Sections for Native Proteomics: Challenges and Opportunities. *J. Proteome Res.* **2022**, *21* (1), 2–8. https://doi.org/10.1021/acs.jproteome.1c00686.

(41) Vallejo, D. D.; Rojas Ramírez, C.; Parson, K. F.; Han, Y.; Gadkari, V. V.; Ruotolo, B. T. Mass Spectrometry Methods for Measuring Protein Stability. *Chem. Rev.* **2022**, *122* (8), 7690–7719.
https://doi.org/10.1021/acs.chemrev.1c00857.

(42) McCabe, J. W.; Shirzadeh, M.; Walker, T. E.; Lin, C.-W.; Jones, B. J.; Wysocki, V. H.; Barondeau, D. P.; Clemmer, D. E.; Laganowsky, A.; Russell, D. H. Variable-Temperature Electrospray Ionization for Temperature-Dependent Folding/Refolding Reactions of Proteins and Ligand Binding. *Anal. Chem.* **2021**, *93* (18), 6924–6931. https://doi.org/10.1021/acs.analchem.1c00870.

(43) Zhou, M.; Lantz, C.; Brown, K. A.; Ge, Y.; Paša-Tolić, L.; Loo, J. A.; Lermyte, F. Higher-Order Structural Characterisation of Native Proteins and Complexes by Top-down Mass Spectrometry. *Chem. Sci.* **2020**, *11* (48), 12918–12936. https://doi.org/10.1039/D0SC04392C.

(44) Brodbelt, J. S.; Morrison, L. J.; Santos, I. Ultraviolet Photodissociation Mass Spectrometry for Analysis of Biological Molecules. *Chem. Rev.* **2020**, *120* (7), 3328–3380. https://doi.org/10.1021/acs.chemrev.9b00440.

(45) Christofi, E.; Barran, P. Ion Mobility Mass Spectrometry (IM-MS) for Structural Biology: Insights Gained by Measuring Mass, Charge, and Collision Cross Section. *Chem. Rev.* **2023**, *123* (6), 2902–2949. https://doi.org/10.1021/acs.chemrev.2c00600.

(46) Young, L. M.; Saunders, J. C.; Mahood, R. A.; Revill, C. H.; Foster, R. J.; Tu, L.-H.; Raleigh, D. P.; Radford, S. E.; Ashcroft, A. E. Screening and Classifying Small-Molecule Inhibitors of Amyloid Formation Using Ion Mobility Spectrometry–Mass Spectrometry. *Nature Chem* **2015**, *7* (1), 73–81. https://doi.org/10.1038/nchem.2129.

(47) Vonderach, M.; Byrne, D. P.; Barran, P. E.; Eyers, P. A.; Eyers, C. E. DNA Binding and Phosphorylation Regulate the Core Structure of the NF-κB P50 Transcription Factor. *J. Am. Soc. Mass Spectrom.* **2019**, *30* (1), 128–138. https://doi.org/10.1007/s13361-018-1984-0.

(48) Polasky, D. A.; Dixit, S. M.; Vallejo, D. D.; Kulju, K. D.; Ruotolo, B. T. An Algorithm for Building Multi-State Classifiers Based on Collision-Induced Unfolding Data. *Anal. Chem.* **2019**, *91* (16), 10407–10412. https://doi.org/10.1021/acs.analchem.9b02650.

(49) Beeston, H. S.; Klein, T.; Norman, R. A.; Tucker, J. A.; Anderson, M.; Ashcroft, A. E.; Holdgate, G. A. Validation of Ion Mobility Spectrometry - Mass Spectrometry as a Screening Tool to Identify Type II Kinase Inhibitors of FGFR1 Kinase. *Rapid Communications in Mass Spectrometry n/a* (n/a), e9130. https://doi.org/10.1002/rcm.9130.

(50) James, V. K.; Sanders, J. D.; Aizikov, K.; Fort, K. L.; Grinfeld, D.; Makarov, A.; Brodbelt, J. S. Expanding Orbitrap Collision Cross-Section Measurements to Native Protein Applications Through Kinetic Energy and Signal Decay Analysis. *Anal. Chem.* **2023**, *95* (19), 7656–7664. https://doi.org/10.1021/acs.analchem.3c00594.

(51) Cong, X.; Liu, Y.; Liu, W.; Liang, X.; Russell, D. H.; Laganowsky, A. Determining Membrane Protein–Lipid Binding Thermodynamics Using Native Mass Spectrometry. *J. Am. Chem. Soc.* **2016**, *138* (13), 4346–4349. https://doi.org/10.1021/jacs.6b01771.

(52) Walker, T. E.; Shirzadeh, M.; Sun, H. M.; McCabe, J. W.; Roth, A.; Moghadamchargari, Z.; Clemmer, D. E.; Laganowsky, A.; Rye, H.; Russell, D. H. Temperature Regulates Stability, Ligand Binding (Mg2+ and ATP), and Stoichiometry of GroEL–GroES Complexes. *J. Am. Chem. Soc.* **2022**, *144* (6), 2667–2678. https://doi.org/10.1021/jacs.1c11341.

(53) Rachel Mehaffey, M.; Ahn, Y.-C.; D. Rivera, D.; W. Thomas, P.; Cheng, Z.; W. Crowder, M.; F. Pratt, R.; Fast, W.; S. Brodbelt, J. Elusive Structural Changes of New Delhi Metallo-β-Lactamase Revealed by Ultraviolet Photodissociation Mass Spectrometry. *Chemical Science* **2020**, *11* (33), 8999–9010. https://doi.org/10.1039/D0SC02503H.

(54) Sipe, S. N.; Lancaster, E. B.; Butalewicz, J. P.; Whitman, C. P.; Brodbelt, J. S. Symmetry of 4-Oxalocrotonate Tautomerase Trimers Influences Unfolding and Fragmentation in the Gas Phase. *J. Am. Chem. Soc.* **2022**, *144* (27), 12299–12309. https://doi.org/10.1021/jacs.2c03564.

(55) Osipiuk, J.; Azizi, S.-A.; Dvorkin, S.; Endres, M.; Jedrzejczak, R.; Jones, K. A.; Kang, S.; Kathayat, R. S.; Kim, Y.; Lisnyak, V. G.; Maki, S. L.; Nicolaescu, V.; Taylor, C. A.; Tesar,

C.; Zhang, Y.-A.; Zhou, Z.; Randall, G.; Michalska, K.; Snyder, S. A.; Dickinson, B. C.; Joachimiak, A. Structure of Papain-like Protease from SARS-CoV-2 and Its Complexes with Non-Covalent Inhibitors. *Nat Commun* **2021**, *12* (1), 743. https://doi.org/10.1038/s41467-021-21060-3.

(56) Sacco, M. D.; Ma, C.; Lagarias, P.; Gao, A.; Townsend, J. A.; Meng, X.; Dube, P.; Zhang, X.; Hu, Y.; Kitamura, N.; Hurst, B.; Tarbet, B.; Marty, M. T.; Kolocouris, A.; Xiang, Y.; Chen, Y.; Wang, J. Structure and Inhibition of the SARS-CoV-2 Main Protease Reveal Strategy for Developing Dual Inhibitors against Mpro and Cathepsin L. *Science Advances* **2020**, *6* (50), eabe0751. https://doi.org/10.1126/sciadv.abe0751.

(57) Higashi-Kuwata, N.; Tsuji, K.; Hayashi, H.; Bulut, H.; Kiso, M.; Imai, M.; Ogata-Aoki, H.; Ishii, T.; Kobayakawa, T.; Nakano, K.; Takamune, N.; Kishimoto, N.; Hattori, S.; Das, D.; Uemura, Y.; Shimizu, Y.; Aoki, M.; Hasegawa, K.; Suzuki, S.; Nishiyama, A.; Saruwatari, J.; Shimizu, Y.; Sukenaga, Y.; Takamatsu, Y.; Tsuchiya, K.; Maeda, K.; Yoshimura, K.; Iida, S.; Ozono, S.; Suzuki, T.; Okamura, T.; Misumi, S.; Kawaoka, Y.; Tamamura, H.; Mitsuya, H. Identification of SARS-CoV-2 Mpro Inhibitors Containing P1' 4-Fluorobenzothiazole Moiety Highly Active against SARS-CoV-2. *Nat Commun* **2023**, *14* (1), 1076. https://doi.org/10.1038/s41467-023-36729-0.

(58) Ma, C.; Xia, Z.; Sacco, M. D.; Hu, Y.; Townsend, J. A.; Meng, X.; Choza, J.; Tan, H.; Jang, J.; Gongora, M. V.; Zhang, X.; Zhang, F.; Xiang, Y.; Marty, M. T.; Chen, Y.; Wang, J. Discovery of Di- and Trihaloacetamides as Covalent SARS-CoV-2 Main Protease Inhibitors with High Target Specificity. *J. Am. Chem. Soc.* **2021**, *143* (49), 20697–20709. https://doi.org/10.1021/jacs.1c08060.

(59) El-Baba, T. J.; Lutomski, C. A.; Kantsadi, A. L.; Malla, T. R.; John, T.; Mikhailov, V.; Bolla, J. R.; Schofield, C. J.; Zitzmann, N.; Vakonakis, I.; Robinson, C. V. Allosteric Inhibition of the SARS-CoV-2 Main Protease: Insights from Mass Spectrometry Based Assays**. *Angewandte Chemie International Edition* **2020**, *59* (52), 23544–23548. https://doi.org/10.1002/anie.202010316.

(60) Butalewicz, J.; Sipe, S.; Juetten, K.; James, V.; Meek, T.; Brodbelt, J. Insights into the Main Protease of SARS-CoV-2: Thermodynamic Analysis, Structural Characterization, and the Impact of Inhibitors. ChemRxiv November 6, 2023. https://doi.org/10.26434/chemrxiv-2023-lgv9f.

(61) Sanders, J. D.; Shields, S. W.; Escobar, E. E.; Lanzillotti, M. B.; Butalewicz, J. P.; James, V. K.; Blevins, M. S.; Sipe, S. N.; Brodbelt, J. S. Enhanced Ion Mobility Separation and Characterization of Isomeric Phosphatidylcholines Using Absorption Mode Fourier Transform Multiplexing and Ultraviolet Photodissociation Mass Spectrometry. *Anal. Chem.* **2022**, *94* (10), 4252–4259. https://doi.org/10.1021/acs.analchem.1c04711.

(62) Blevins, M. S.; Juetten, K. J.; James, V. K.; Butalewicz, J. P.; Escobar, E. E.; Lanzillotti, M. B.; Sanders, J. D.; Fort, K. L.; Brodbelt, J. S. Nanohydrophobic Interaction Chromatography Coupled to Ultraviolet Photodissociation Mass Spectrometry for the Analysis of Intact Proteins in Low Charge States. *J. Proteome Res.* **2022**, *21* (10), 2493–2503. https://doi.org/10.1021/acs.jproteome.2c00450.

(63) Juetten, K. J.; Brodbelt, J. S. MS-TAFI: A Tool for the Analysis of Fragment Ions Generated from Intact Proteins. *J. Proteome Res.* **2023**, *22* (2), 546–550. https://doi.org/10.1021/acs.jproteome.2c00594.

(64) Shin, D.; Mukherjee, R.; Grewe, D.; Bojkova, D.; Baek, K.; Bhattacharya, A.; Schulz, L.; Widera, M.; Mehdipour, A. R.; Tascher, G.; Geurink, P. P.; Wilhelm, A.; van der Heden van Noort, G. J.; Ovaa, H.; Müller, S.; Knobeloch, K.-P.; Rajalingam, K.; Schulman, B. A.; Cinatl, J.; Hummer, G.; Ciesek, S.; Dikic, I. Papain-like Protease Regulates SARS-CoV-2 Viral Spread and Innate Immunity. *Nature* **2020**, *587* (7835), 657–662. https://doi.org/10.1038/s41586-020-2601-5.

(65) Békés, M.; van der Heden van Noort, G. J.; Ekkebus, R.; Ovaa, H.; Huang, T. T.; Lima, C. D. Recognition of Lys48-Linked Di-Ubiquitin and Deubiquitinating Activities of the SARS Coronavirus Papain-like Protease. *Molecular Cell* **2016**, *62* (4), 572–585. https://doi.org/10.1016/j.molcel.2016.04.016.

(66) O'Brien, J. P.; Li, W.; Zhang, Y.; Brodbelt, J. S. Characterization of Native Protein Complexes Using Ultraviolet Photodissociation Mass Spectrometry. *J. Am. Chem. Soc.* **2014**, *136* (37), 12920–12928. https://doi.org/10.1021/ja505217w.

(67) Nowak, Ł.; Krajewski, W.; Dejnaka, E.; Małkiewicz, B.; Szydełko, T.; Pawlak, A. Ubiquitin-Specific Proteases as Potential Therapeutic Targets in Bladder Cancer—In Vitro Evaluation of Degrasyn and PR-619 Activity Using Human and Canine Models. *Biomedicines* **2023**, *11* (3), 759. https://doi.org/10.3390/biomedicines11030759.

(68) Lin, W.-C.; Chiu, Y.-L.; Kuo, K.-L.; Chow, P.-M.; Hsu, C.-H.; Liao, S.-M.; Dong, J.-R.; Chang, S.-C.; Liu, S.-H.; Liu, T.-J.; Hsu, F.-S.; Wang, K.-C.; Lin, Y.-C.; Chang, C.-C.; Huang, K.-Y. Anti-Tumor Effects of Deubiquitinating Enzyme Inhibitor PR-619 in Human Chondrosarcoma through Reduced Cell Proliferation and Endoplasmic Reticulum Stress-Related Apoptosis. *Am J Cancer Res* **2023**, *13* (7), 3055–3066.

(69) James, V. K.; Sanders, J. D.; Aizikov, K.; Fort, K. L.; Grinfeld, D.; Makarov, A.; Brodbelt, J. S. Expanding Orbitrap Collision Cross-Section Measurements to Native Protein Applications Through Kinetic Energy and Signal Decay Analysis. *Anal. Chem.* **2023**, *95* (19), 7656–7664. https://doi.org/10.1021/acs.analchem.3c00594.

Insert Table of Contents artwork here